Simulated Density Currents beneath Embedded Stratified Layers

ROBERT B. SEIGEL AND SUSAN C. VAN DEN HEEVER

Department of Atmospheric Science, Colorado State University, Fort Collins, Colorado

(Manuscript received 4 October 2011, in final form 29 December 2011)

ABSTRACT

The goal of this research is to investigate the impacts of a stably stratified layer embedded within a neutrally stratified environment on the behavior of density currents in an effort to extend the environmental regimes examined by Liu and Moncrieff. Such environments frequently support severe weather events. To accomplish this goal, nonhydrostatic numerical model experiments are performed in which the strength and height of the embedded stably stratified layer within a neutrally stratified environment are varied. The 1-km-deep stable layer base is varied between 1, 2, and 3 km AGL. Additionally, the strength of the stable layer is systematically varied between Brunt–Väisälä frequencies of 0.006, 0.012, and 0.018 s^{-1}, following the methodology of Liu and Moncrieff. The model and grid setup are also similar to that of Liu and Moncrieff, utilizing the Arakawa C grid, leapfrog advection, a Robert–Asselin filter, and grid spacing of 100 and 50 m in the horizontal and vertical directions, respectively. Results show that the height of the density current decreases and the propagation speed increases with stronger and lower stable layers, provided that the stable layer is sufficiently thin so as to not act as a gravity wave ducting layer. As the strength of the stable layer increases and the height of this layer decreases, the horizontal pressure gradient driving the density current increases, resulting in faster propagation speeds. Such results have implications for cold pool propagation into more stable environments.

1. Introduction

Cold pools have long been qualitatively compared to density currents; however, Charba (1974) was the first to quantitatively relate an observed thunderstorm outflow to a laboratory-produced density current. Since then there have been numerous other studies (Droegemeier and Wilhelmson 1985, 1987; Xu 1992; Liu and Moncrieff 1996a,b, 2000, hereafter LM2000; Simpson 1997; Xue 2002; Engerer et al. 2008), both observational and modeling, which have focused on the generation and complexities of these atmospheric density currents. This study aims to build on previous theoretical density current research to further our knowledge of cold pool characteristics within observed atmospheric environments.

It has been previously demonstrated that in addition to shear (Xu 1992; Liu and Moncrieff 1996a,b; Xu et al. 1996; Xue 2000), the stability of the ambient environment plays a large role in the propagation and structure of density currents (Thorpe et al. 1980; Droegemeier and Wilhelmson 1985; Bischoff-Gauss and Gross 1989; Raymond and Rotunno 1989; Haase and Smith 1989; Jin et al. 1996; Liu and Moncrieff 1996a,b; LM2000). Theoretical modeling studies of density currents propagating within complex thermodynamic environments have been performed in order to replicate realistic atmospheric environments. Thorpe et al. (1980) simulated density currents propagating within a neutral environment beneath a deep stably stratified environment, thus representing a daytime boundary layer. Conversely, Jin et al. (1996) examined density currents within stably stratified environments beneath a neutral layer, representing the nighttime boundary layer. Additionally, LM2000 used a numerical model to analyze how the density current head height and propagation speed are modulated within ambient stratification regimes that represent typical atmospheric environments. In their investigation they simulated three environmental regimes: (i) a stably stratified layer underneath deep, neutrally stratified flow; (ii) a neutrally stratified layer underlying a deep, stably stratified flow; and (iii) a continuously stratified atmosphere. They find that case (i) decreases the height of the density current

Corresponding author address: Robert B. Seigel, 1371 Campus Delivery Drive, Fort Collins, CO 80523.
E-mail: rseigel@atmos.colostate.edu

DOI: 10.1175/JAS-D-11-0255.1

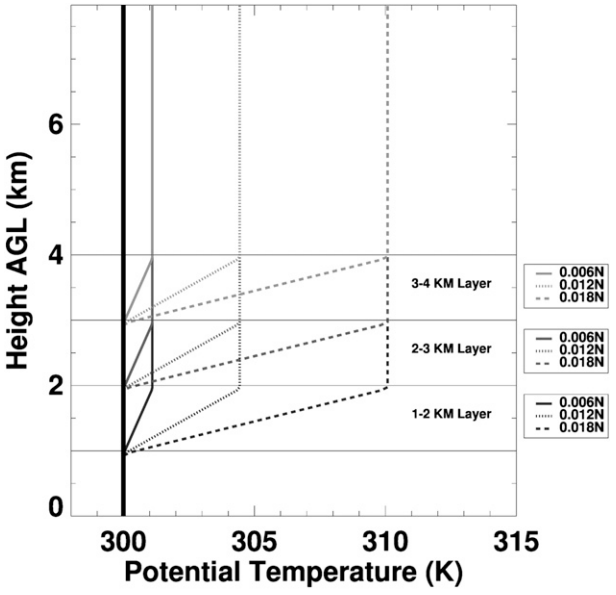

FIG. 1. Base-state potential temperature profile for each sensitivity simulation. The stable layers vary between 1–2 (dark gray), 2–3 (medium gray), and 3–4 km AGL (light gray). The strength of the stable layers vary between $N = 0.006$ (solid), 0.012 (dotted), and 0.018 s^{-1} (dashed). The control experiment is depicted by the thick black line.

and increases the propagation speed with increasing stratification; case (ii) reduces density current height and its propagation speed with increasing stratification; and case (iii) demonstrates similar responses to case (ii).

This paper focuses on testing a fourth regime in which a neutrally stratified atmosphere contains an embedded, vertically thin, stably stratified layer (Fig. 1), an environment that is typically associated with severe convection. While the regime examined in this paper is principally different than each experiment of LM2000, this regime is most closely related to the LM2000 case (ii) (hereafter referred to as LM2000ii), because for both of these experiments, the density current propagates within the neutrally stratified layer below the stable layer, and the layer overlying the density current is stably stratified. This provides similar environmental controls on the dynamics of the density current. The sole difference between the regime examined here and LM2000ii is the depth of the overlying stably stratified layer, in that LM2000ii contains a deeply stratified layer from 1 km AGL to model top (15 km) whereas this research examines the impacts of a vertically thin (1-km) stratified layer. The inclusion of the vertically thin stable layer requires an additional neutral layer above the stable layer. Thus the atmospheric environment investigated here is one of a neutral layer, overlaid by a thin stably stratified layer, which in turn is overlaid by a neutral layer as shown in Fig. 1. This setup allows for an investigation of the sensitivity of the density current characteristics on the depth and strength of the stable layer, and therefore extends the LM2000 study to further storm environments.

The environmental regime investigated here is often observed in pre–squall line environments where high convective available potential energy (CAPE) and a convective inhibition (CINH) layer exist (Schmidt and Cotton 1989; Smith and Gall 1989; Bryan and Parker 2010). An example of this can be seen in Fig. 8b of Bryan and Parker (2010), which was generated using radiosonde data 74 min before the passage of a squall line. In Fig. 8b of Bryan and Parker (2010) three distinct environmental layers are evident that can be characterized by 1) low-level neutral stratification from the surface to ~800 hPa, 2) shallow stable stratification from ~800 to ~700 hPa, and 3) upper-level neutral stratification from ~700 to ~500 hPa. These three environmental layers are synonymous with the environment simulated in this experiment (Fig. 1). Additionally, supercell tornadogenesis is often observed to occur within environments that contain CINH and high CAPE (Davies 2004). Ziegler et al. (2010) investigated the role that stable layers atop neutrally stratified boundary layers play in supercell tornadogenesis. They modeled a tornadic supercell that propagated within a relatively cold, yet neutrally stratified, boundary layer beneath a vertically thin stable layer. In their modeling experiments it was found that an accelerated retrograding motion of the forward-flank outflow boundary was instrumental in the demise of the supercell. The overlying stable layer could have influenced the propagation speed of the outflow boundary.

Because severe weather is often observed within environments containing a thin stably stratified layer, it is important to obtain an understanding of cold pool propagation within such environments (Moncrieff and Liu 1999). Therefore, this study examines the role a thin stable layer embedded within a neutrally stratified environment plays on cold pool structure and propagation characteristics by performing sensitivity experiments in which the height and strength of a 1-km-deep stable layer are varied. It is hypothesized that altering the depth from a deeply stratified atmosphere (as in LM2000ii) to a vertically thin stratified layer (this experiment) will reverse the trend of the cold pool propagation speed seen in LM2000ii, and that propagation speeds will increase with increasing layer stability. The following section briefly describes the model used for this study and the experiment setup. The third section presents and discusses the results of this study and the fourth section provides a brief summary of the experiment results.

2. Methods

The numerical model used for the experiments conducted here includes the same model physics as described by Droegemeier and Wilhelmson (1987) and is thus similar to the model used by LM2000 (Clark 1977). The quasi-compressible, nonhydrostatic, anelastic equations employed are (Droegemeier and Wilhelmson 1987) as follows:

$$\frac{\partial u}{\partial t} = -u\frac{\partial u}{\partial x} - w\frac{\partial u}{\partial z} - c_{p_d}\overline{\theta}\frac{\partial \pi'}{\partial x} + \frac{\partial}{\partial x}\left(K_{mx}\frac{\partial u}{\partial x}\right) + \frac{\partial}{\partial z}\left(K_{mz}\frac{\partial u}{\partial z}\right), \quad (1)$$

$$\frac{\partial w}{\partial t} = -u\frac{\partial w}{\partial x} - w\frac{\partial w}{\partial z} - c_{p_d}\overline{\theta}\frac{\partial \pi'}{\partial x} + g\frac{\theta'}{\overline{\theta}} + \frac{\partial}{\partial x}\left(K_{mx}\frac{\partial w}{\partial x}\right) + \frac{\partial}{\partial z}\left(K_{mz}\frac{\partial w}{\partial z}\right), \quad (2)$$

$$\frac{\partial \theta'}{\partial t} = -u\frac{\partial \theta'}{\partial x} - w\frac{\partial \theta'}{\partial z} - w\frac{\partial \overline{\theta}}{\partial z} + \frac{\partial}{\partial x}\left(K_{hx}\frac{\partial \theta'}{\partial x}\right) + \frac{\partial}{\partial z}\left(K_{hz}\frac{\partial \theta'}{\partial z}\right), \quad (3)$$

$$\frac{\partial \pi'}{\partial t} = -\frac{\overline{c}_s^2}{\overline{\rho}c_{p_d}\overline{\theta}^2}\left(\frac{\partial \overline{\rho}\theta u}{\partial x} + \frac{\partial \overline{\rho}\theta w}{\partial z}\right) + \frac{\partial}{\partial x}\left(K_{hx}\frac{\partial \pi'}{\partial x}\right) + \frac{\partial}{\partial z}\left(K_{hz}\frac{\partial \pi'}{\partial z}\right), \quad (4)$$

where a prime denotes the perturbation from the base state and an overbar denotes the base-state variable, which is only a function of height. Equations (1)–(4) are discretized for this limited-domain model to prognose u (horizontal wind), w (vertical wind), θ (temperature), and π (Exner perturbation function). In Eq. (4), c_{p_d} is the specific heat capacity for dry air and $\overline{c}_s$ is the speed of sound, which has been set to 100 m s^{-1} following the methodology of Droegemeier and Wilhelmson (1987). The coefficients K_{mx} and K_{mz} are the horizontal and vertical computational diffusion coefficients for the momentum equations, and K_{hx} and K_{hz} are the horizontal and vertical computational diffusion coefficients for the scalar equations.

The 2D numerical grid utilizes the Arakawa C staggering and is 4000 points × 160 points in the horizontal and vertical directions, respectively. Grid spacing of 100 m in the horizontal and 50 m in the vertical has been utilized in order to keep the model setup as similar as possible to that of LM2000. This results in a grid domain size of 400 km × 8 km. Sensitivity testing was performed on the vertical depth of the domain and a higher model top did not change the solution. The time step used is 0.125 s and the model is run for 2000 s. The second-order leapfrog advection scheme and a Robert–Asselin filter are utilized. Periodic lateral boundary conditions are applied; however, the numerical domain used for all of these simulations is sufficiently large that the density current does not interact with the lateral boundaries during the entire analysis time period. The model top is a rigid lid with no mass transport through the upper boundary and the bottom boundary is a free-slip boundary, similar to LM2000.

This simple model allows for the isolation of key dynamical processes in the analysis of density currents; however, the grid spacing employed has been shown to have errors of up to 4% when compared against a reference solution of 25-m grid spacing (Straka et al. 1993), and the slab-symmetric coordinate system used here is known to slightly underperform an axisymmetric coordinate system when simulating density currents (Straka and Anderson 1993). In spite of the weak potential errors this may introduce, this grid spacing and coordinate system are utilized in order to maintain model setups as similar to LM2000 as possible, thereby reducing the uncertainties in output associated with differences in the models used.

The density current is initialized by allowing a cold bubble to descend within an initially motionless base-state environment. The cold bubble, shaped like the top half of an ellipse with the semimajor axis located at the surface, contains a maximum thermal perturbation of −15 K that is sine-smoothed to a horizontal radius of 4 km and a vertical depth of 6 km. Once time integration commences, the negatively buoyant air within the bubble descends and spreads out laterally, generating two identical density currents moving in opposite directions. The density currents exhibit maximum thermal perturbations of −6 K, which compare well with observed thunderstorm outflow thermal perturbations (Engerer et al. 2008).

Ten simulations of the cold bubble are performed. The control experiment contains an isentropic atmosphere with no stably stratified layer. In the nine sensitivity experiments the height AGL and strength of the embedded stably stratified layer are varied through modifications to the base-state θ profile (Fig. 1). All stable layers are 1 km deep, but their base heights vary between 1, 2, and 3 km. The strength of the stable layer is defined following LM2000 and makes use of a constant Brunt–Väisälä frequency within the layer. Using the same values as LM2000ii, the strength of the stable layers is varied between 0.006, 0.012, and 0.018 s^{-1}. As the depth of the initial cold bubble is

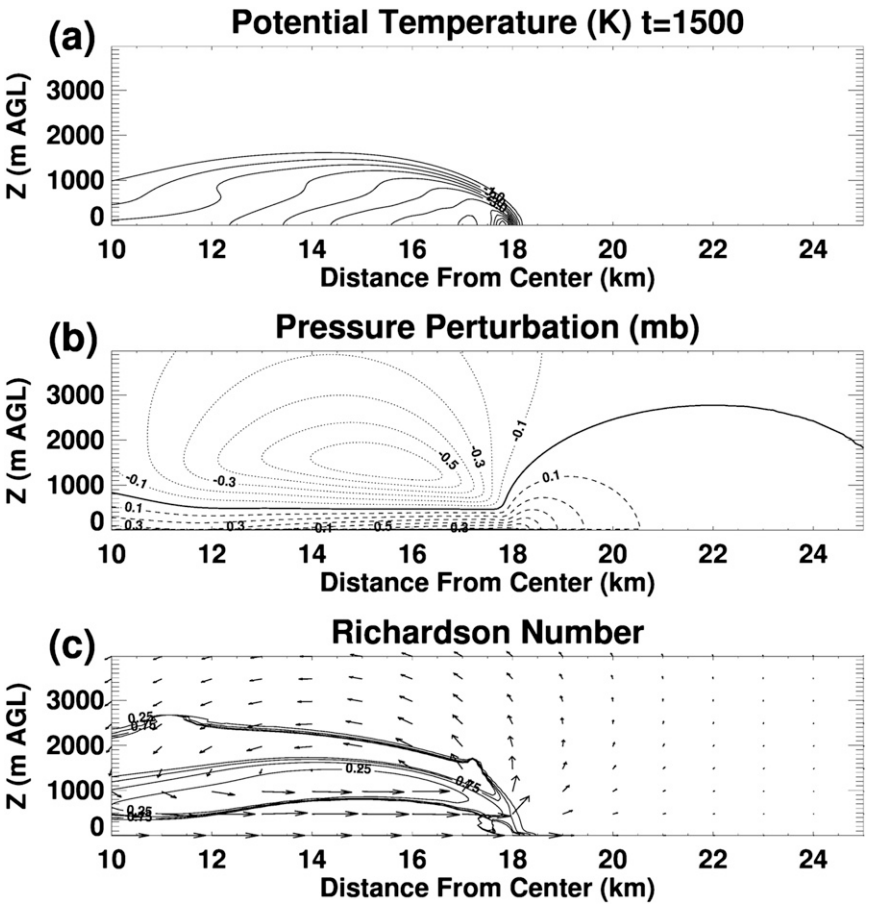

FIG. 2. Density current generated from cold bubble for the control experiment after 1500 s. (a) Potential temperature perturbation contoured at 0.5-K interval. (b) Pressure perturbation for 0-mb contour (solid), positive perturbation (dashed), and negative perturbation (dotted) at 0.1-mb interval. (c) System-relative flow (vectors) and Richardson number at 0.25 interval.

greater than the height of the stable layer, the stable layer is located 8 km away from the cold bubble to allow for steady density current formation prior to layer interaction. The 8-km distance has been determined to be the spinup distance of the density current based on the control simulation, which took 10 min of time integration for the gust front to reach that location. This spinup time period is similar to that found by Wolfson (1983) through numerical simulations of downbursts. Wolfson (1983) found that it takes approximately 9 min after downdraft touchdown for downbursts to show differences when simulated within a neutral versus a stable boundary layer. Additionally, the imposed stable layer is linearly smoothed over 8 km in the lateral direction to avoid abrupt impacts to the density current. Supplementary simulations were performed with our model and the setup of LM2000ii, the results (not shown) of which successfully replicated those shown in LM2000, thus ensuring consistency between the models and their setups.

3. Results and discussion

a. Control experiment

As previously stated, the left- and right-moving portions of the density current are mirror images of one another and the background environment is initially motionless. Therefore the analysis in this section is performed only with regards to the right-moving density current. Also, as this paper builds on LM2000, analysis similar to theirs is presented here in order to facilitate comparisons.

To illustrate the model's capability in generating a realistic density current from a cold bubble, Fig. 2 shows the density current for the control experiment (i.e., uniform neutral stratification) after 1500 s. This time has

TABLE 1. Experiment naming convention.

Stable layer location (km AGL)	$N = 0.006$	$N = 0.012$	$N = 0.018$
1–2	06N1km	12N1km	18N1km
2–3	06N2km	12N2km	18N2km
3–4	06N3km	12N3km	18N3km

TABLE 2. Cold pool propagation speed (m s^{-1}) for each simulation.

Simulation	$N = 0.006$	$N = 0.012$	$N = 0.018$
1–2 km AGL	11.00	11.83	12.33
2–3 km AGL	10.83	11.17	11.17
3–4 km AGL	10.67	11.83	11.83
Control	10.67	10.67	10.67

been chosen because the density current's location is beneath the embedded stable layers in the sensitivity experiments at this time. In Fig. 2a the potential temperature perturbation shows the overall shape of the density current. This is characterized by an elevated head region behind the gust front with a shallower wake of cold air. The maximum temperature perturbation, which is defined by the difference between the local temperature and the base-state temperature (Fig. 1), is about −6 K and agrees well with observations of continental cold pools (Engerer et al. 2008).

As a result of the hydrostatic forces associated with the cold air within the density current, a positive pressure perturbation (Fig. 2b), which is defined by the difference between the local pressure and the base-state pressure, is seen that is characteristic of classic density current models (Simpson 1969, 1997; Goff 1976; Xue 2002). Additionally, a positive pressure perturbation is seen ahead of the density current that is a result of nonhydrostatic forces from increased convergence near the gust front (LM2000). Within the rotational head and above the density current (Figs. 2b,c), nonhydrostatic effects are contributing to the negative pressure perturbations and are also in keeping with classical density current models (Simpson 1969; Goff 1976) and LM2000. In association with the large vertical shear at the top of the density current, Kelvin–Helmholtz instability is often observed and also appears in these experiments (Fig. 2c). This is evident in both the potential temperature field with the overturning of potential temperature surfaces (Fig. 2a) and the Richardson number field with values less than 0.25 (Fig. 2c; Miles 1961; Jin et al. 1996). The following section investigates the effects of an embedded stable layer on the described density current.

b. Sensitivity experiments

As previously described, the sensitivity experiments are designed to investigate the impacts of an embedded 1-km-deep, stably stratified layer within a neutrally stratified environment on the characteristics of a density current. In these experiments, the naming convection of which is given in Table 1, the strength of the stable layer is varied between $N = 0.006$, 0.012, and 0.018 s^{-1} and the base height of the stable layer between 1, 2, and 3 km. The density current propagation speed is calculated by following the surface −0.5-K potential temperature perturbation at the gust front. It is apparent from Table 2 that with the exception of two experiments, the stable layer acts to increase propagation speed and decrease the density current head height (Fig. 3). The two anomalous experiments (18N2km and 18N3km) will be further investigated below. Figure 3 shows maximum vertical velocity, head height, and maximum pressure perturbation associated with the density current for each experiment in order to illustrate the dynamical trends resulting from the various stable layers.

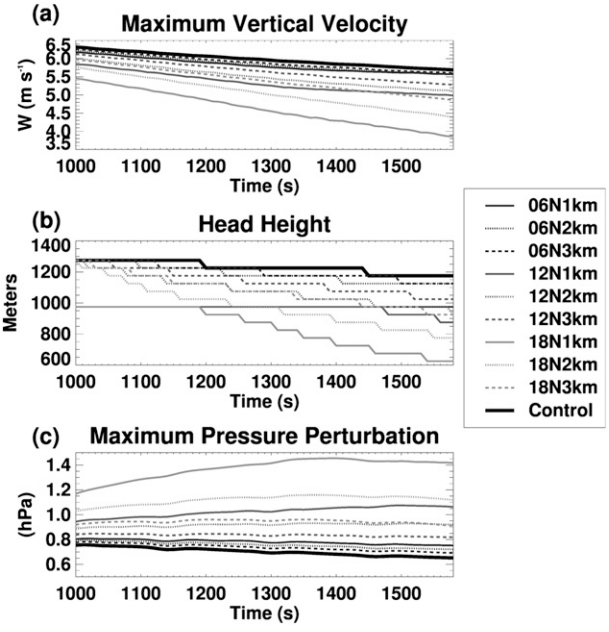

FIG. 3. Density current trends for the nine sensitivity experiments described in the text and the control experiment. Each experiment consists of a stable layer with depth of 1–2 (solid), 2–3 (dotted), or 3–4 km AGL (dashed) and a strength of $N = 0.006$ (dark gray), 0.012 (medium gray), or 0.018 s^{-1} (light gray). The control experiment is depicted by the thick black contour. (a) Maximum vertical velocity associated with the gust front, (b) density current head height, and (c) maximum pressure perturbation.

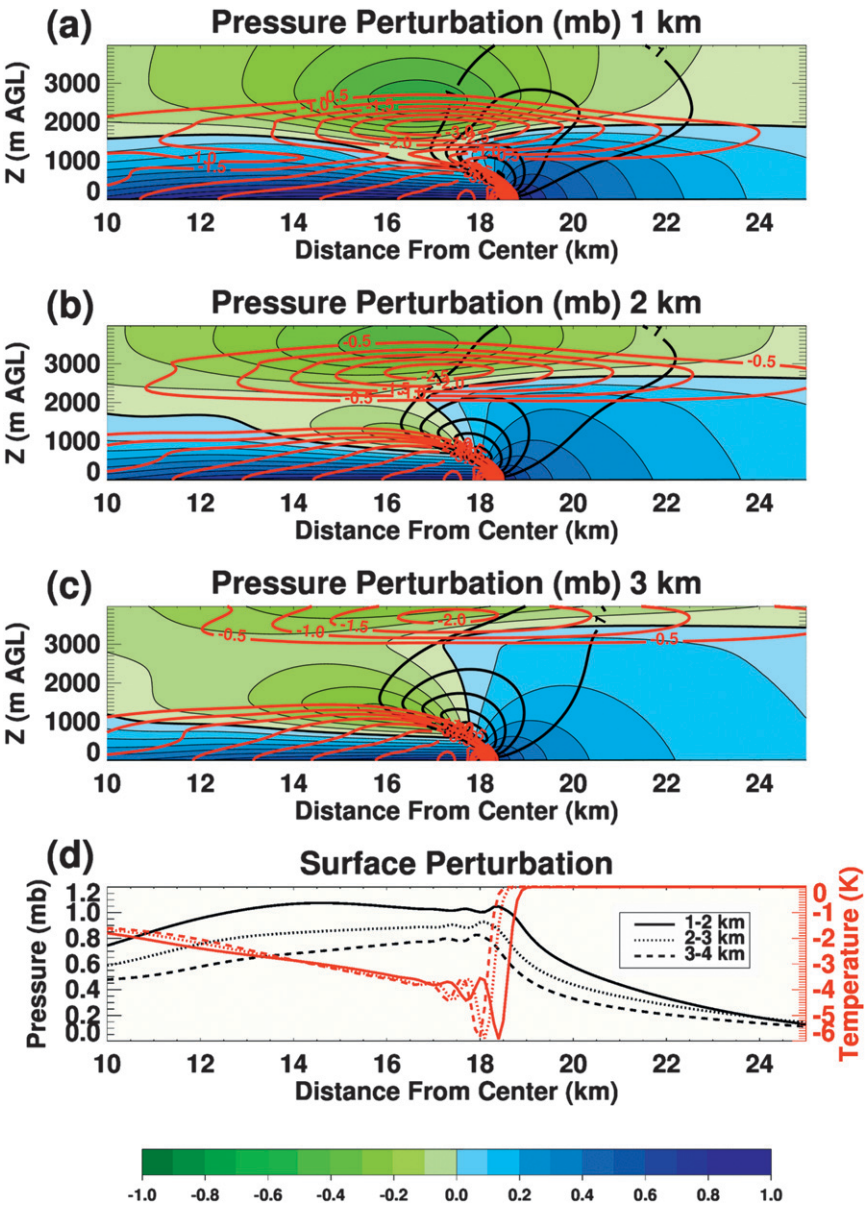

FIG. 4. Density current after 1500 s and associated temperature, pressure, and vertical velocity fields for the three experiments with the $N = 0.012\ s^{-1}$ stable layer. Positive pressure perturbation at 0.1-mb interval (blue shading), negative pressure perturbation at 0.1-mb interval (green shading), temperature perturbation at 0.5-K interval (red contours), and vertical velocity at 1 m s^{-1} interval (black contours) are shown for the (a) 1–2, (b) 2–3, and (c) 3–4 km AGL experiments. (d) The surface temperature (red) and pressure (black) perturbations for the three experiments.

It can be seen that for all of the experiments the maximum vertical velocity (Fig. 3a), which is located near the gust front (see Fig. 4), decreases with the addition of a stable layer, with the most significant reductions occurring in association with the stronger and lower stable layers. As described by LM2000, this trend can be explained by the stabilization effect where a stronger and lower stable layer suppresses the vertical displacement of air lifted by the density current due to negative buoyancy. This increased suppression of vertical motion with stronger and lower stable layers also reduces head heights (Fig. 3b).

As shown in Fig. 3c, the maximum pressure perturbations also exhibit a distinct trend, whereby the stronger and lower stable layers increase the maximum pressure perturbation—all of which occur at the

surface just behind the outflow boundary. To explain these trends, Figs. 4a–c show the pressure perturbations, temperature perturbations, and vertical velocity values associated with the density current for all three $N = 0.012\ s^{-1}$ stable-layer simulations (12N1km, 12N2km, and 12N3km) after 1500 s. The $N = 0.012\ s^{-1}$ simulations have been chosen to illustrate the process under moderate stability. Also depicted in Fig. 4d are the surface values of pressure and temperature perturbation for the three simulations. As the height of the stable layer is increased, the suppression of the mechanical lifting ahead of the density current is reduced. As previously stated, this trend is due to the stabilization effect where 12N1km (Fig. 4a) has the stable layer more closely tied to the vertical motion and hence a more dramatic reduction of vertical velocity. However, as the collocation of stratification and larger vertical velocity values exists in 12N1km (Fig. 4a) as compared with 12N2km (Fig. 4b) and 12N3km (Fig. 4c), in which the stable layer is higher up, stronger adiabatic ascent occurs within the stable layer. This stronger mechanically forced ascent gives rise to the larger temperature perturbation within the stable layer (<-3.5 K) in 12N1km (Fig. 4a) as compared with 12N3km (<-2 K) (Fig. 4c). Because of hydrostatic forces, the stronger temperature perturbation for the 1-km stable layer experiment (Fig. 4a) simultaneously increases the surface pressure and results in a stronger pressure gradient (Fig. 4d) that forces faster density current propagation (Table 2). Similar analyses can be used to explain the trend of a stronger stable layer yielding faster propagation (Table 2) and a lower head height (Fig. 3). The maximum difference in propagation speed found between experiments is about 1.67 m s^{-1}, which is substantial when applying this difference to realistic time scales of squall lines. For example, using 5 h as an approximate time scale for a squall line, this difference gives rise to a roughly 30-km variation in distance traveled by the cold pool.

The reversal in propagation speed between this experiment and LM2000ii can be attributed to gravity waves. In LM2000ii, the authors attribute the decrease in propagation speed with increasing stratification to gravity wave trapping. In their case, as the overlying deep stratification increases, the gravity wave propagation speed increases but remains locked to the density current and results in stronger pressure generation out ahead of the density current. This weakens the surface pressure gradient and therefore reduces the propagation speed with increasing stratification. For the experiments presented here, the gravity waves dissipate too quickly to affect the downstream pressure perturbations. The dissipation can be explained by gravity wave ducting theory (Lindzen and Tung 1976). Because of the three-layer regime examined here (i.e., neutral to stable to neutral stratification), the vertically thin stable layer could potentially act as a gravity wave duct. According to Lindzen and Tung (1976), certain criteria must be met in order for the stable layer to act as a ducting layer. One such criterion states that the duct must be sufficiently thick to accommodate one-quarter of the vertical wavelength of the wave (Lindzen and Tung 1976). A simple calculation can be made to determine if the stable layer is sufficiently thick to duct gravity wave energy generated by the density current using

$$D = \frac{(c - \overline{u})\pi}{2N}, \tag{5}$$

where c is the horizontal phase speed, $\overline{u}$ is the environmental wind relative to the direction of wave propagation, N is the Brunt–Väisälä frequency, and D is the depth of the stably stratified layer. For these experiments, $\overline{u}$ is zero, N ranges between 0.006, 0.012, and 0.018 s^{-1}, and c has been numerically calculated for each simulation (Table 2). Using these values, the minimum depth for each experiment that can allow gravity wave ducting is shown in Table 3. From this, it can be seen that with the exception of the two anomalous experiments previously mentioned (18N2km and 18N3km), all the experiments require a ducting depth D greater than 1 km, the depth of the stable layer investigated here. This indicates that for the experiments that exhibit propagation speed increasing with increasing stability, the gravity wave energy cannot be sufficiently ducted and the gravity wave energy dissipates, thereby allowing the surface pressure field to be relatively unaffected by propagating gravity waves. Conversely, as soon as the ducting depth decreases to less than 1 km, gravity wave energy can be more efficiently ducted. This results in the ability of the ducted gravity wave to more significantly impact the below-pressure field. Once this occurs, the stable layer begins to affect the density current in a manner similar to LM2000ii where the surface pressure gradient is reduced and the density current propagation slows down. This can be seen in Table 3 for 18N2km and 18N3km where both ducting depths are less than 1 km and the propagation speed (Table 2) remained constant, rather than increasing.

TABLE 3. Approximate minimum depth (m) for each simulation to allow gravity wave ducting (Lindzen and Tung 1976).

Simulation	$N = 0.006$	$N = 0.012$	$N = 0.018$
1–2 km AGL	2880	1548	1076
2–3 km AGL	2836	1462	974
3–4 km AGL	2793	1418	945

As such, the trends in propagation speed seen with the other seven sensitivity experiments in this study do not apply to 18N2km and 18N3km because the embedded stable layer acted as a ducting layer.

4. Conclusions

A two-dimensional nonhydrostatic model has been used to perform a theoretical study that examines the impact of an embedded stable layer within a neutrally stratified environment on density current structure and propagation. Such regimes are typical of severe weather environments containing high CAPE and some CINH. Testing this regime extends the previous experiments of LM2000. By systematically varying the height and strength of a 1-km-deep embedded stable layer it has been shown that with stronger and lower stable layers the density current propagation increases and the density current head height decreases, provided the depth of the stable layer is too thin to prevent gravity wave ducting.

This experiment setup most closely resembles the second regime of LM2000 in which they investigated density current characteristics in a neutrally stratified layer beneath a deep stably stratified layer. In both this experiment and LM2000ii, the density current propagates within the neutrally stratified layer and below the stable layer, thus making this experiment dynamically comparable to LM2000ii. LM2000 found that deep upper-level stratification reduces both the density current head height and propagation speed. While the thin embedded stable layer in our experiments also reduces the density current head height, the propagation speed increases with increasing stratification. LM2000 relate the decrease in density current propagation speed in their experiment to gravity wave trapping that causes a reduction in the horizontal pressure gradient. However, in the simulations described here it is shown that if the upper-level stratification is sufficiently shallow such that it cannot act as a ducting layer, then the horizontal pressure gradient behind the cold pool boundary can increase, causing faster gust front propagation. These findings are important for the understanding of cold pool–driven phenomenon, especially for squall line and supercell propagation into environments containing shallow but strong inversions at the top of the boundary layer.

Acknowledgments. This work was funded jointly by the Department of Defense Center for Geosciences/Atmospheric Research at Colorado State University under Cooperative Agreement W911NF-06-2-0015 with the Army Research Laboratory and the National Science Foundation under Grant NSFATM-0820557. The authors also thank the two reviewers, whose helpful comments improved the content of this manuscript.

REFERENCES

Bischoff-Gauss, I., and G. Gross, 1989: Numerical studies on cold fronts. Part I: Gravity flows in a neutral and stratified atmosphere. *Meteor. Atmos. Phys.,* **40,** 150–158.

Bryan, G. H., and M. D. Parker, 2010: Observations of a squall line and its near environment using high-frequency rawinsonde launches during VORTEX2. *Mon. Wea. Rev.,* **138,** 4076–4097.

Charba, J., 1974: Application of gravity current model to analysis of squall-line gust front. *Mon. Wea. Rev.,* **102,** 140–156.

Clark, T. L., 1977: A small-scale dynamic model using a terrain-following coordinate transformation. *J. Comp. Phys.,* **24,** 186–215.

Davies, J. M., 2004: Estimations of CIN and LFC associated with tornadic and nontornadic supercells. *Wea. Forecasting,* **19,** 714–726.

Droegemeier, K. K., and R. B. Wilhelmson, 1985: Three-dimensional numerical modeling of convection produced by interacting thunderstorm outflows. Part II: variations in vertical wind shear. *J. Atmos. Sci.,* **42,** 2404–2414.

——, and ——, 1987: Numerical simulation of thunderstorm outflow dynamics. Part I: Outflow sensitivity experiments and turbulence dynamics. *J. Atmos. Sci.,* **44,** 1180–1210.

Engerer, N. A., D. J. Stensrud, and M. C. Coniglio, 2008: Surface characteristics of observed cold pools. *Mon. Wea. Rev.,* **136,** 4839–4849.

Goff, R. C., 1976: Vertical structure of thunderstorm outflows. *Mon. Wea. Rev.,* **104,** 1429–1440.

Haase, S. P., and R. K. Smith, 1989: The numerical simulation of atmospheric gravity currents. Part II: Environments with stable layers. *Geophys. Astrophys. Fluid Dyn.,* **46,** 35–51.

Jin, Y., S. E. Koch, Y.-L. Lin, F. M. Ralph, and C. Chen, 1996: Numerical simulations of an observed gravity current and gravity waves in an environment characterized by complex stratification and shear. *J. Atmos. Sci.,* **53,** 3570–3588.

Lindzen, R. S., and K.-K. Tung, 1976: Banded convective activity and ducted gravity waves. *Mon. Wea. Rev.,* **104,** 1602–1617.

Liu, C.-H., and M. W. Moncrieff, 1996a: A numerical study of the effects of ambient flow and shear on density currents. *Mon. Wea. Rev.,* **124,** 2282–2303.

——, and ——, 1996b: An analytical study of density currents in sheared, stratified fluids including the effects of latent heating. *J. Atmos. Sci.,* **53,** 3303–3312.

——, and ——, 2000: Simulated density currents in idealized stratified environments. *Mon. Wea. Rev.,* **128,** 1420–1437.

Miles, J. W., 1961: On the stability of heterogeneous shear flows. *J. Fluid Mech.,* **10,** 496–508.

Moncrieff, M. W., and C. Liu, 1999: Convection initiation by density currents: Role of convergence, shear, and dynamical organization. *Mon. Wea. Rev.,* **127,** 2455–2464.

Raymond, D. J., and R. Rotunno, 1989: Response of a stably stratified flow to cooling. *J. Atmos. Sci.,* **48,** 2830–2837.

Schmidt, J. M., and W. R. Cotton, 1989: A high plains squall line associated with severe surface winds. *J. Atmos. Sci.,* **46,** 281–302.

Simpson, J., 1969: A comparison between laboratory and atmospheric density currents. *Quart. J. Roy. Meteor. Soc.,* **95,** 758–765.

——, 1997: *Gravity Currents in the Environment and the Laboratory*. John Wiley, 244 pp.

Smith, W. P., and R. L. Gall, 1989: Tropical squall lines of the Arizona monsoon. *Mon. Wea. Rev.,* **117,** 1553–1569.

Straka, J. M., and J. R. Anderson, 1993: Extension and application of a local, minimum aliasing method to multidimensional problems in limited-area domains. *Mon. Wea. Rev.,* **121,** 2903–2918.

——, R. B. Wilhelmson, L. J. Wicker, J. R. Anderson, and K. K. Droegemeier, 1993: Numerical solutions of a non-linear density current: A benchmark solution and comparisons. *Int. J. Numer. Methods Fluids,* **17,** 1–22.

Thorpe, A. J., M. J. Miller, and M. W. Moncrieff, 1980: Dynamical models of two-dimensional downdraughts. *Quart. J. Roy. Meteor. Soc.,* **106,** 463–484.

Wolfson, M. M., 1983: Understanding and predicting microbursts. Ph.D. dissertation, Massachusetts Institute of Technology, 303 pp.

Xu, Q., 1992: Density currents in shear flows—A two-fluid model. *J. Atmos. Sci.,* **49,** 511–524.

——, M. Xue, and K. K. Droegemeier, 1996: Numerical simulation of density currents in sheared environments within a vertically confined channel. *J. Atmos. Sci.,* **53,** 770–786.

Xue, M., 2000: Density currents in two-layer shear flows. *Quart. J. Roy. Meteor. Soc.,* **126,** 1301–1320.

——, 2002: Density currents in shear flows: Effects of rigid lid and cold-pool internal circulation, and application to squall line dynamics. *Quart. J. Roy. Meteor. Soc.,* **128,** 47–73.

Ziegler, C. L., E. R. Mansell, J. M. Straka, D. R. MacGorman, and D. W. Burgess, 2010: The impact of spatial variations of low-level stability on the life cycle of a simulated supercell storm. *Mon. Wea. Rev.,* **138,** 1738–1766.